CEPT1-Mediated Phospholipogenesis Regulates Endothelial Cell Function and Ischemia-Induced Angiogenesis Through PPARα

Mohamed A. Zayed,[1,2,3,4] Xiaohua Jin,[1] Chao Yang,[1] Larisa Belaygorod,[1] Connor Engel,[1] Kshitij Desai,[1] Nikolai Harroun,[1] Omar Saffaf,[1] Bruce W. Patterson,[5] Fong-Fu Hsu,[6] and Clay F. Semenkovich[6]

Diabetes 2021;70:549–561 | https://doi.org/10.2337/db20-0635

De novo phospholipogenesis, mediated by choline-ethanolamine phosphotransferase 1 (CEPT1), is essential for phospholipid activation of transcription factors such as peroxisome proliferator–activated receptor α (PPARα) in the liver. Fenofibrate, a PPARα agonist and lipid-lowering agent, decreases amputation incidence in patients with diabetes. Because we previously observed that CEPT1 is elevated in carotid plaque of patients with diabetes, we evaluated the role of CEPT1 in peripheral arteries and PPARα phosphorylation (Ser12). CEPT1 was found to be elevated in diseased lower-extremity arterial intima of individuals with peripheral arterial disease and diabetes. To evaluate the role of *Cept1* in the endothelium, we engineered a conditional endothelial cell (EC)–specific deletion of *Cept1* via induced *VE-cadherin-CreERT2*–mediated recombination (*Cept1Lp/LpCre*$^{+}$). *Cept1Lp/LpCre*$^{+}$ ECs demonstrated decreased proliferation, migration, and tubule formation, and *Cept1Lp/LpCre*$^{+}$ mice had reduced perfusion and angiogenesis in ischemic hind limbs. Peripheral ischemic recovery and PPARα signaling were further compromised by streptozotocin-induced diabetes and ameliorated by feeding fenofibrate. *Cept1* endoribonuclease-prepared siRNA decreased PPARα phosphorylation in ECs, which was rescued with fenofibrate but not PC16:0/18:1. Unlike *Cept1Lp/LpCre*$^{+}$ mice, *Cept1Lp/LpCre*$^{+}$*Ppara*$^{-/-}$ mice did not demonstrate hind-paw perfusion recovery after feeding fenofibrate. Therefore, we demonstrate that CEPT1 is essential for EC function and tissue recovery after ischemia and that fenofibrate rescues CEPT1-mediated activation of PPARα.

Lipids for mammalian metabolism are derived from two main sources: diet and endogenous de novo synthesis (1–3). De novo phospholipogenesis is the process whereby excess carbohydrates and proteins are converted into phospholipids (4–6). Choline-enthanolamine phosphotransferase 1 (CEPT1), a 47-kDa membrane-bound protein that catalyzes the terminal step of the Kennedy pathway (2), is encoded by the *Cept1* gene (7) and responsible for phosphatidylcholine (PC) and phosphatidylethanolamine (PE) production (1,2,8). PC and PE are the dominant phospholipids in mammalian cells and are essential for a myriad of cellular processes, including organelle/plasma membrane structure and integrity (9), lipoprotein secretion (10), and DNA and protein synthesis (11). A growing body of evidence demonstrates that disruption of phospholipogenesis is associated with a variety of human conditions, including obesity, metabolic syndrome, and diabetes (1,3,9,12–14).

Peroxisome proliferator–activated receptor α (PPARα) is a ligand-activated transcription factor that belongs to the superfamily of nuclear hormone receptors (15). In the circulatory system, PPARα is present in endothelial cells (ECs), where it can be activated by both exogenous pharmacological fibrate drugs like fenofibrate, clofibrate, and

[1]Section of Vascular Surgery, Department of Surgery, Washington University School of Medicine in St. Louis, St. Louis, MO
[2]Division of Molecular Cell Biology, Washington University School of Medicine in St. Louis, St. Louis, MO
[3]Department of Biomedical Engineering, McKelvey School of Engineering, Washington University in St. Louis, St. Louis, MO
[4]VA St. Louis Health Care System, St. Louis, MO
[5]Center for Human Nutrition, Department of Medicine, Washington University School of Medicine in St. Louis, St. Louis, MO
[6]Division of Endocrinology, Metabolism and Lipid Research, Department of Medicine, Washington University School of Medicine in St. Louis, St. Louis, MO

Corresponding author: Mohamed A. Zayed, zayedm@wustl.edu

Received 15 June 2020 and accepted 12 November 2020

This article contains supplementary material online at https://doi.org/10.2337/figshare.13229129.

gemfibrozil and endogenous ligands such as the CEPT1-derived phospholipid derivative PC16:0/18:1 (16). Activated PPARα can alter intracellular lipid metabolism through multiple mechanisms, including stimulation of enzymes that promote metabolism of fatty acids, such as acyl-CoA oxidase (ACOX1), carnitine palmitoyl transferase (CPT1), and medium-chain acyl-CoA dehydrogenase (17).

Individuals with type 2 diabetes (T2D) have a higher prevalence of hypertriglyceridemia and microvascular arterial occlusive disease and higher risk of foot wounds and limb amputations (18–21). It is estimated that somewhere in the world, an amputation is performed every 30 s in individuals with diabetes (22). The Fenofibrate Intervention and Event Lowering in Diabetes (FIELD) study is the only clinical trial to date demonstrating that treatment with fenofibrate (a PPARα agonist and lipid-lowering agent) significantly reduced lower-extremity amputations in individuals with diabetes (23). It remains unclear how fenofibrate confers its beneficial limb-preserving effects. We hypothesized that the effect of fenofibrate is in part related to intracellular lipid metabolism, and we tested this hypothesis by evaluating the effect of fenofibrate on CEPT1-mediated activation of PPARα in the endothelium.

RESEARCH DESIGN AND METHODS

Human Selection and Arterial Intima Procurement

The human portion of this study was performed using an institutional review board–approved study protocol, and all study patients provided written informed consent before participation. From April 2016 to November 2016, 31 patients with and without chronic T2D undergoing lower-extremity amputation because of advanced nonsalvageable peripheral arterial disease (PAD) were prospectively enrolled in a tissue biobank for collection of arterial segments from their amputated limbs. Immediately after the amputation in the operating room, tibial arterial segments from the lower legs were harvested en bloc, placed in cold saline solution, maintained on ice, and immediately transferred to the laboratory for isolation of the arterial intima and further analysis. Arterial intima was subdivided into maximally (Max) and minimally (Min) diseased arterial segments as previously described (24). Arterial intima segments were embedded in paraffin, snap frozen in liquid nitrogen and stored at −80°C, or preserved for RNA isolation.

Animal Regulations

All housing, breeding, and experimental procedures involving mice were conducted in accordance with national guidelines and regulations and approved by the local university institutional animal care and use committee.

Generation of Mouse Models

Inducible knockdown of CEPT1 in the mouse vascular endothelium was facilitated by crossing *VE-cadherin-CreERT2* mice (25,26) with CEPT1-floxed mice (*Loxp* sites flanking exon 3 of the *Cept1* gene; *Cept1Lp/Lp*) (Supplementary Fig. 1*A* and *B*). Littermates at least 8 weeks of age received tamoxifen (TMX) treatment (five daily i.p. injections at 1 mg per mouse) to induce *Cre* expression and endothelial *Cept1* gene knockdown.

Isolation of Primary ECs

Hearts and lungs of *Cept1Lp/Lp Cre*$^{-}$, *Cept1Lp/Lp Cre*$^{+}$, *Ppara*$^{-/-}$, and *Ppara*$^{+/+}$ mice ∼1–3 months of age were dissected from the mouse mediastinum and prepared for EC isolation as previously described (27). Organs were gently minced, collagenase digested, and strained. The resulting cell suspension underwent positive cell sorting using PECAM-1 (BD Biosciences, San Jose, CA) anti-rat IgG-conjugated magnetic beads (Invitrogen, Carlsbad, CA). Isolated cells were plated in tissue culture flasks and cultured in growth media. Heart (MHECs) and lung ECs (MLECs) were then purified with a second round of positive cell sorting using either PECAM-1 or ICAM-2 (BD Biosciences) coated magnetic beads. The remaining ECs were cultured for up to two to three passages.

EC Function Assays

Cell proliferation and death were evaluated using BrdU incorporation assay and anti-DNA/histone ELISA, respectively. In a 96-well culture format, 1×10^4 ECs were seeded per well, followed by serum starvation for at least 6 h. Growth media was then added, and proliferation and death were independently evaluated after 24 h according to manufacturer's instructions (Roche, Indianapolis, IN) using a multiwell spectrophotometer at 450 nm as previously described (27,28). Each assay was repeated in triplicate.

EC migration was evaluated using a monolayer EC migration assay as previously described (27,28). Monolayer scratches were serially evaluated at 0, 3, 6, and 16 h, and percentage of wound area closure was measured using ImageJ software. Each condition was repeated in triplicate.

EC tubule formation was evaluated using a 48-well culture format as previously described (27). Cells on the growth factor–reduced Matrigel were then incubated in the presence of growth media or basal media supplemented with 25 μmol/L fenofibrate. Three random 20× images were collected for each condition at baseline and at 2, 4, and 6 h postincubation. Each assay was repeated in triplicate.

EC Culture, Lysis, Western Blotting, and Immunohistochemistry

Human umbilical vein ECs (HUVECs) were maintained in EBM culture media according to manufacturer's instructions (Cambrex, East Rutherford, NJ). MHECs and MLECs were isolated in isolation media (i.e., high-glucose DMEM with 20% FBS, 20 units/mL penicillin/streptomycin antibiotic [Gibco, Carlsbad, CA], and 20 units/L heparin [Sigma]) and maintained in highly supplemented growth media. Cells were serum starved in basal media. For acute knockdown of *Cept1*, ECs were cultured to at least 60% confluence and then treated with 5 μmol/L TMX for 48 h.

ECs were then lysed in modified CHAPS buffer (20 mmol/L HEPES, pH 7.4, 0.15 mol/L NaCl, 10 mmol/L CHAPS, 50 mmol/L NaF, 10 mmol/L β-glycerophosphate, 1 mmol/LM each of $CaCl_2$ and $MgCl_2$, and Protease Inhibitors Cocktail Set III [Calbiochem, San Diego, CA]) on ice for at least 30 min.

For hind-limb muscle tissue, ~50 mg of ischemic hind-limb adductor or gastrocnemius muscle tissue was homogenized in cold RIPA Lysis Buffer System (sc-24948; Santa Cruz Biotechnology) containing Halt Protease and Phosphatase Inhibitor Cocktail (78442; Thermo Fisher Scientific).

Total protein from ECs and muscle tissue was determined using a Bradford protein assay, loaded onto SDS-PAGE, and transferred to polyvinylidene fluoride membranes for Western blotting. Proteins were detected with rabbit anti-CEPT1 (20496–1-AP; Proteintech Group), anti-PPARα, rabbit antiphospho-PPARα (Ser 12; PA1820; Life Technologies Corp.), rabbit anti-ACOX1 (10957–1-AP; Proteintech), and mouse anti-CPT1a (66039–1-Ig; Proteintech) antibodies. Rabbit anti–caveolin-1 (ab2910; Abcam Biotechnology) was used for Western blot loading controls. Band densitometry analysis was performed using ImageJ software as previously described (27,28). Band densities were averaged across triplicate blots and expressed as ratios relative to protein loading control or nonphosphorylated total protein.

For immunostaining, HUVECs were fixed with 100% methanol and serially washed with PBS; 2% BSA blocking agent was added for 1 h at room temperature. Immunostaining was then performed using primary antiphospho-PPARα (Ser12) 1:200 or rabbit anti-CEPT1 antibody 1:50. Primary antibody was detected with a secondary antibody donkey anti-rabbit IgG labeled with Alexa Fluor 555 1:400 (A31572; Thermo Fisher Scientific), followed by DAPI staining. Imaging assessments were performed using a DFC 3000 G Leica Microsystems inverted fluorescent microscope, and staining was quantified using ImageJ software (29).

Murine Hind-Limb Ischemia

Cept1Lp/LpCre^{-}, *Cept1Lp/LpCre*$^{+}$, *Ppara*$^{-/-}$, and *Cept1Lp/LpCre*$^{+}$*Ppara*$^{-/-}$ mice were either maintained on a regular diet for 12 weeks or initiated on a fenofibrate diet at 6 weeks of age. At 8 weeks of age, mice were also treated with or without streptozotocin (STZ) (0.1 mg/g of body weight administered i.p. once daily for five consecutive days) to induce hyperglycemia and a diabetes-like phenotype (28,30). At 12 weeks of age, all mice received TMX (0.05 mg/g of body weight administered i.p. once daily for five consecutive days) to induce *Cre* expression acute knockout of endothelial *Cept1*. At 10 days after *Cept1* knockout, unilateral hind-limb ischemia (HLI) was performed as previously described (28). At 7 days post-HLI, mouse hind-limb or hind-paw Doppler perfusion, skeletal muscle histology, and microvessel density were evaluated.

Real-time PCR

RNA was purified from HUVECs, MLECs, and human arterial intima tissue as previously described (24). Target mRNA was quantified by real-time PCR using specified primer sets (designed to span introns, not react with genomic DNA, and validated with quantitative PCR melting curve analysis) (Supplementary Table 1) and Applied Biosystems PowerUp SYBR Green Master Mix (A25742; Thermo Fischer Scientific). Samples were evaluated using the 7500 Fast Real-Time PCR System (Applied Biosystems) and analyzed using Fast System Software (Applied Biosystems). Threshold cycle (Ct) values were normalized to either *RPL32* mRNA (for human EC and tissue analysis) or *RPL34* mRNA (for murine EC analysis) and expressed as fold change relative to the mean Ct value of the control group using the Δ Ct method (31).

Endoribonuclease-Prepared siRNA Construction and Transfection of HUVECs

Endoribonuclease-prepared siRNA (esiRNA) targeting *Cept1* and esiRNA^{-} (*Gfp*) and esiRNA^{+} controls (*Kif11*) was designed and synthesized (#EHU064851, #EHUEGFP, #EHU019931; Sigma-Aldrich). HUVECs (passages 3–5) were plated and cultured with antibiotic free EGM-2 media (CC-3302; Lonza) for 24 h to achieve 40% monolayer confluence. HUVECs were then transfected with esiRNA at 160 pg/μL and transfection reagent Lipofectamine 2000 (13778075; Thermo Fisher Scientific) for up to 36 h. Cells were then starved for 2 h using EBM-2 media (CC-3156; Lonza) and treated with or without 50 μmol/L fenofibrate (F6020; Sigma-Aldrich) for 90 min or 50 μmol/L PC16:0/18:1 (PC34:1; most abundant mammalian PC; #20962, Cayman Chemical), PC18:0/18:2 (PC36:2; second most abundant mammalian PC; #850468, Avanti Polor Lipids), and PC14:0 (nonnaturally occurring PC used for experimental internal standard; #850345, Avanti Polor Lipids) for 2 h. Cells were then evaluated by immunostaining, lipid mass spectrometry, and protein and RNA content analyses between esiRNA conditions.

Electrospray Ionization Mass Spectrometry

Lipid extracts from arterial intima specimens and ECs were analyzed by direct injection electrospray ionization mass spectrometry using a Thermo Vantage triple-quadruple mass spectrometer (San Jose, CA) and an Accela 1250 UPLC system operated via the Xcalibur operating system (24). Structures for all phospholipids were identified using a multiple-stage linear ion trap that was operated at a low-energy collision-induced dissociation and high-resolution mass spectrometry. Phospholipid structural assignments were made as described (24,32–35). Phospholipid content was evaluated relative to internal standard controls as previously described (24).

Mass Spectrometry Phospholipidomic Data Analysis

The mass spectrometry–derived lipid mass spectrum for arterial intima and EC samples was performed as

previously described (24). This analysis included 54 PC-related species (including 23 PCs), 16 alkyl ether PCs (aPCs), and 11 sphingomyelins (Supplementary Table 2) and 22 PE-related species, including 12 PEs and 11 plasmenyl PEs (pPEs) (Supplementary Table 3).

Unilateral Femoral Artery Ligation, Laser Doppler Perfusion Imaging, and Appearance and Use Score Assessments

Ligation, imaging, and use scores were determined as described with some modifications (27). Limb appearance was independently graded on a scale of 0–4 (4 = digit/foot autoamputation, 3 = severe discoloration/gangrene, 2 = moderate discoloration, 1 = mild discoloration, 0 = normal appearance). Limb use was independently graded on a scale of 0–3 (3 = foot dragging, 2 = no foot dragging but no plantar flexion, 1 = abnormal plantar flexion, 0 = normal foot and leg function).

Ischemic Gastrocnemius Muscle Atrophy and Microvascular Capillary Density

Seven days after femoral artery ligation, mice were administered a ketamine (80 mg/kg) and xylazine (10 mg/kg) cocktail. Cold PBS with heparin (10 units/mL) was injected into the heart, and peripheral adductor and gastrocnemius muscles were then harvested for subsequent protein analysis or fixed and paraffin embedded as previously described (28). For each muscle specimen, representative 10-μm sections were obtained and stained with hematoxylin-eosin or labeled with Alexa Fluor 594–conjugated *Griffonia simplicifolia* isolectin-1-B4 1:100 (Invitrogen). Five 20× images were collected for each section from each mouse genotype. Using ImageJ, muscle atrophy and microvascular capillary density were quantified as described (27,28).

Statistical Analysis

Tukey multiple comparison one-way ANOVA was used to evaluate differences in *cept1* between Max and Min arterial intima segments and *Cept1Lp/Lp Cre*$^{-}$ and *Cept1Lp/Lp Cre*$^{+}$ EC proliferation and cell death. Tukey multiple comparison two-way ANOVA was used to evaluate differences in EC tubule sprout formation and migration. Sidak multiple comparison one-way ANOVA was used to evaluate differences in hind-paw Doppler perfusion. Unpaired two-tailed Student *t* test was used to evaluate differences in gene expression in ECs, CEPT1/PPARα/CPT1a/ACOX1 protein content, phospho-PPARα fluorescent intensity in ECs, impact of PC18:0/18:2 and PC16:0/18:1 on phospho-PPARα, and hind-limb collaterals. Unpaired two-tailed Student *t* test was also used to evaluate differences in PCs and PEs in arterial intima segments and MLECs. Unpaired two-tailed Student *t* test with Welch correction was used to evaluate differences in hind-limb Doppler perfusion, relative muscle fiber size, and relative microvessel density. We considered $P < 0.05$ to be significant.

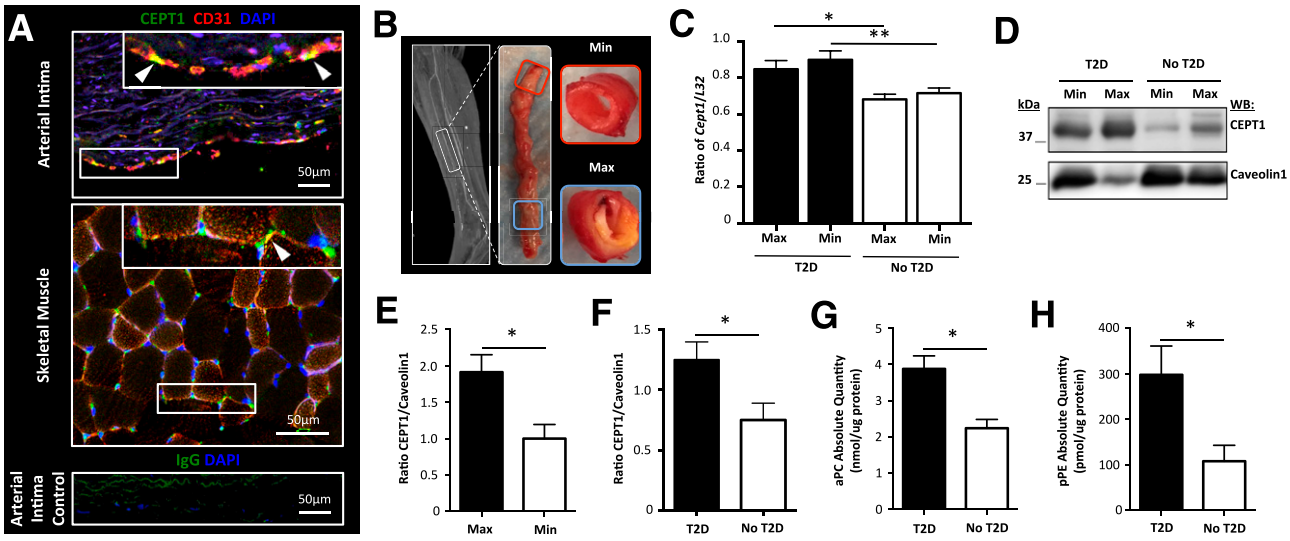

Figure 1—CEPT1 is localized to endothelium and is elevated in the intima of diseased peripheral arteries. *A*: CEPT1 colocalizes with CD31 along the intima endothelial layer of nondiseased aorta. CEPT1 also colocalizes with CD31 in microvascular structures in skeletal muscle tissue (inserts original magnification 1.5×). Arterial intima staining control with IgG secondary antibody demonstrates minimal background staining. *B*: Min and Max diseased peripheral arterial intima segments were procured from lower extremities of patients with severe PAD, with or without T2D, who were undergoing amputation. *C*: Real-time PCR analysis demonstrates higher *Cept1* expression in Max and Min diseased arterial segments of patients with diabetes ($n = 7$ with T2D; $n = 15$ with no T2D). *D*: Representative Western blot demonstrates higher CEPT1 content in Min and Max arterial intima segments of a patient with diabetes. Caveolin-1 blot is a representative loading control. *E*: CEPT1 content is higher in Max diseased arterial intima segments ($n = 12$ patients). *F*: CEPT1 content is also higher in patients with known clinical history of T2D (16 with T2D; 8 with no T2D). *G* and *H*: Mass spectrometry phospholipidomic analysis demonstrated higher aPC content (*G*) and pPE content (*H*) in the arterial intima of patients with T2D ($n = 14$ with T2D; $n = 14$ with no T2D). *$P < 0.05$; **$P < 0.01$. WB, Western blot.

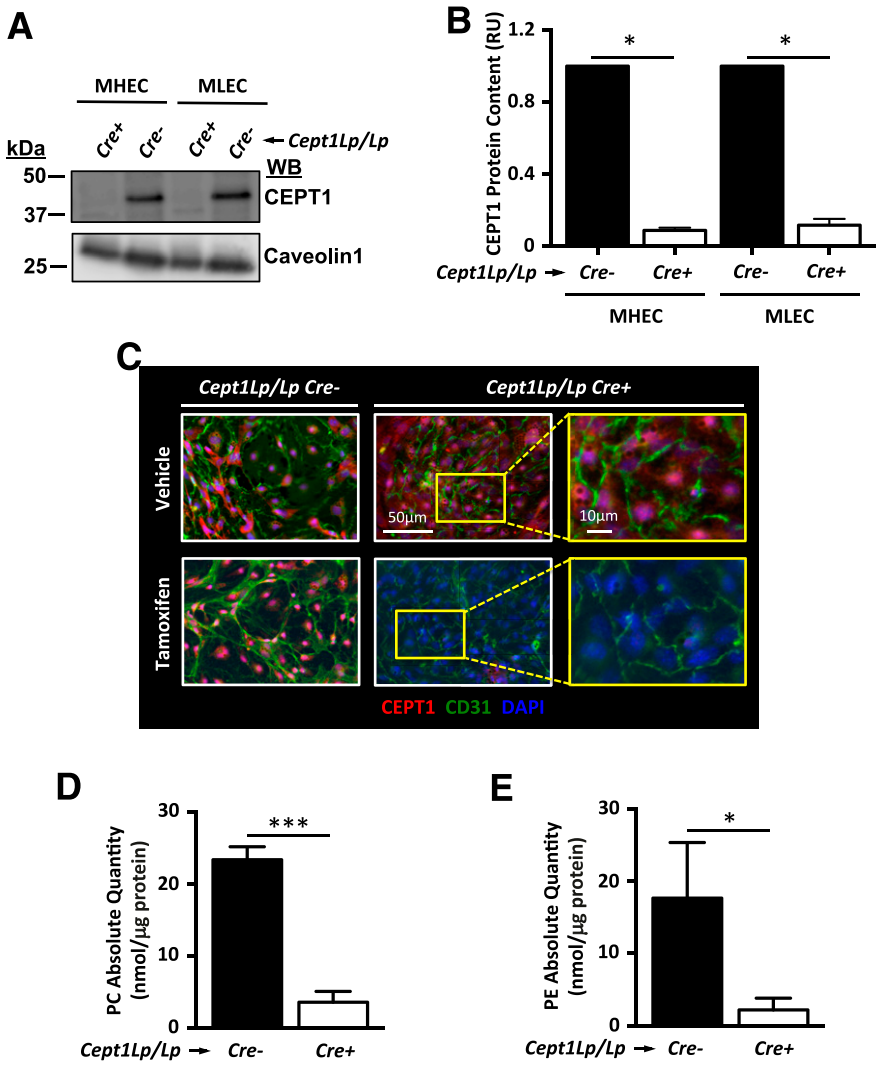

Figure 2—Conditional knockout of *Cept1* in murine endothelium alters phospholipid profile. *A*: Representative Western blot (WB) demonstrates dramatically decreased CEPT1 content in MHECs and MLECs isolated from *Cept1Lp/LpCre*$^{+}$ mice. *B*: Quantitative of three independent Western blots demonstrates significant decrease in CEPT1 protein content in MHECs and MLECs isolated from *Cept1Lp/LpCre*$^{+}$ mice. *C*: Immunostaining of MLECs demonstrates decreased cytoplasmic CEPT1 content after TMX treatment to facilitate *Cre*-medicated recombination and knockout of *Cept1*. *D* and *E*: Mass spectrometry phospholipidomic analysis demonstrated lower PC content (*D*) and PE content (*E*) in *Cept1Lp/LpCre*$^{-}$ and *Cept1Lp/LpCre*$^{+}$ MLECs ($n = 3$ per analysis). *$P < 0.05$; ***$P < 0.001$. RU, relative unit.

Error was presented as SEM. Both sexes were evaluated in human and murine studies and analyzed accordingly.

Data and Resource Availability

The data sets generated and/or analyzed during the current study are available from the corresponding author upon reasonable request.

RESULTS

CEPT1 Protein Content Is Elevated in the Intima of Patients With T2D and PAD

In 31 patients with advanced nonsalvageable lower-extremity PAD, we observed that a majority had cardiovascular risk factors, including hyperlipidemia (74.2%), hypertension (90.3%), and former/current smoking (83.9%) (Supplementary Table 4). Demographics were similar between patients with and without T2D, and none of the patients were taking oral fibrates or fish oil supplements. Vascular immunostaining demonstrated that CEPT1 was present in the endothelial layer of nondiseased macroarterial intima as well as in the microcapillary structures of lower-extremity skeletal muscles (Fig. 1*A*). Arterial intima of Max and Min diseased arterial segments from individuals with PAD (Fig. 1*B*) demonstrated higher *Cept1* expression in individuals with T2D (Fig. 1*C*). Similarly, Max diseased arterial intima tended to have increased expression of *Ppara* and downstream PPARα-activated β-fatty acid oxidation genes *Acox1* and *Cpt1a* (Supplementary Fig. 2). No significant differences were observed between male and female patients (Supplementary Table 5). Similarly,

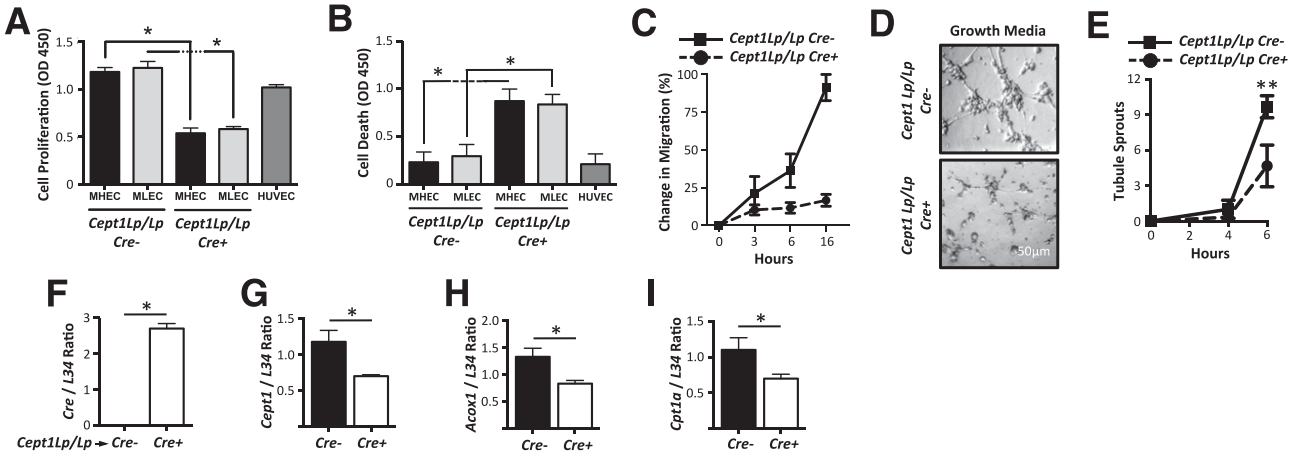

Figure 3—Reduced function and altered gene expression in *Cept1Lp/LpCre*$^{+}$ ECs. *A*: Proliferation of MHECs and MLECs isolated from *Cept1Lp/LpCre*$^{-}$ and *Cept1Lp/LpCre*$^{+}$ mice over 24 h ($n = 3$ per condition). *B*: Cell death of isolated MHECs and MLECs over 24 h ($n = 3$ per condition). *C*: Isolated MHEC monolayer migration over 16 h ($n = 3$ per condition). *D*: Representative images of *Cept1Lp/LpCre*$^{-}$ and *Cept1Lp/LpCre*$^{+}$ MLEC formation of tubules after 6 h of incubation on Matrigel. *E*: *Cept1Lp/LpCre*$^{-}$ and *Cept1Lp/LpCre*$^{+}$ MLEC tubule formation over 6 h ($n = 3$ per condition). *F–I*: *Cept1Lp/LpCre*$^{+}$ MLECs demonstrate robust *Cre* expression (*F*), reduced *Cept1* (*G*), reduced *Acox1* (*H*), and reduced *Cpt1a* (*I*) ($n = 3$ per condition). OD, optical density. $^{*}P < 0.05$; $^{**}P < 0.01$.

we observed 49% higher CEPT1 protein content in Max arterial segments (Fig. 1*D* and *E*) and 37% higher content in arterial segments isolated from individuals with T2D (Fig. 1*D* and *F*). As in human tissue, CEPT1 protein content was also higher in the aortic tissue of *db/db* compared with $^{+/+}$ mice (Supplementary Fig. 3). Arterial intima of individuals with T2D demonstrated higher CEPT1-derived aPC and pPE phospholipids (Fig. 1*G* and *H*).

Conditional Knockdown of Cept1 in the Endothelium

Cept1Lp/LpCre^{+} mice treated with TMX demonstrated successful *Cre* recombination of *Cept1* gene in heart, aorta, and lung tissue (Supplementary Fig. 1*C*). Primary MHECs and MLECs isolated from *Cept1Lp/LpCre*$^{+}$ mice demonstrated a >95% decrease in CEPT1 protein content (Fig. 2*A* and *B*). TMX-induced *Cre*-mediated recombination led to a dramatic reduction of CEPT1 in the cytoplasm and nucleus of *Cept1Lp/LpCre*$^{+}$ MLECs (Fig. 2*C*). PC and PE content were also significantly reduced in *Cept1Lp/LpCre*$^{+}$ MLECs compared with *Cept1Lp/LpCre*$^{-}$ MLECs (Fig. 2*D* and *E*). Supplementary Figure 4 and Supplementary Tables 3 and 4 provide a summary of all PC and PE species analyzed using electrospray ionization mass spectrometry.

Cept1 Knockdown Decreases EC Function and PPARα Activation

Compared with *Cept1Lp/LpCre*$^{-}$, *Cept1Lp/LpCre*$^{+}$ MHECs and MLECs demonstrated significantly reduced proliferation (Fig. 3*A*) and increased cell death (Fig. 3*B*). *Cept1Lp/LpCre*$^{+}$ MHECs demonstrated significantly reduced cell migration over 16 h in growth media (Fig. 3*C* and Supplementary Fig. 5). Similarly, *Cept1Lp/LpCre*$^{+}$ MLECs demonstrated significantly reduced tubule formation over 6 h in growth media (Fig. 3*D* and *E*). *Cept1Lp/LpCre*$^{+}$ MLECs also demonstrated robust *Cre* expression (Fig. 3*F*), reduced *Cept1* expression (Fig. 3*G*), and decreased *Acox1* and *Cpt1a* expression (Fig. 3*H* and *I*).

Recovery of Cept1Lp/LpCre^{+} Ischemic Hind Limbs After STZ and Fenofibrate Treatments

Cept1Lp/LpCre^{-} and *Cept1Lp/LpCre*$^{+}$ mice were divided across four experimental cohorts (Fig. 4*A*). No significant differences were observed with regard to the sex (Supplementary Table 6) and body weight of *Cept1Lp/LpCre*$^{-}$ and *Cept1Lp/LpCre*$^{+}$ mice that received either fenofibrate diet or STZ treatment (Supplementary Fig. 6*A* and *B*). Both *Cept1Lp/LpCre*$^{-}$ and *Cept1Lp/LpCre*$^{+}$ mice that were maintained on a regular or fenofibrate diet and treated with STZ developed severe hyperglycemia (Supplementary Fig. 6*C* and *D*).

All experimental groups received unilateral HLI, and Doppler perfusion was evaluated at 1 week post-HLI (Fig. 4*A*). *Cept1Lp/LpCre*$^{+}$ mice demonstrated significantly reduced ischemic hind-limb Doppler perfusion compared with *Cept1Lp/LpCre*$^{-}$ mice (Fig. 4*B* and *C*). Perfusion reduction in the ischemic hind limbs of *Cept1Lp/LpCre*$^{+}$ mice was even more noticeable in the STZ-treated cohort (Fig. 4*B* and *C*). Interestingly, fenofibrate seemed to ameliorate hind-limb perfusion in *Cept1Lp/LpCre*$^{+}$ mice that were treated with or without STZ (Fig. 4*D* and *E*).

To evaluate the effect of STZ and/or fenofibrate on ischemic hind limbs of *Cept1Lp/LpCre*$^{+}$ mice, we also evaluated hind-limb microvascular capillary density and extent of resultant skeletal muscle damage. We observed that gastrocnemius muscle angiogenesis microvessel density was significantly reduced in the ischemic hind limbs of *Cept1Lp/LpCre*$^{+}$ mice maintained on either a regular or fenofibrate diet (Fig. 4*F–H*). No difference was observed in arterial collateral density (arteriogenesis) in the ischemic hind-limb adductor muscle segments of *Cept1Lp/LpCre*$^{+}$

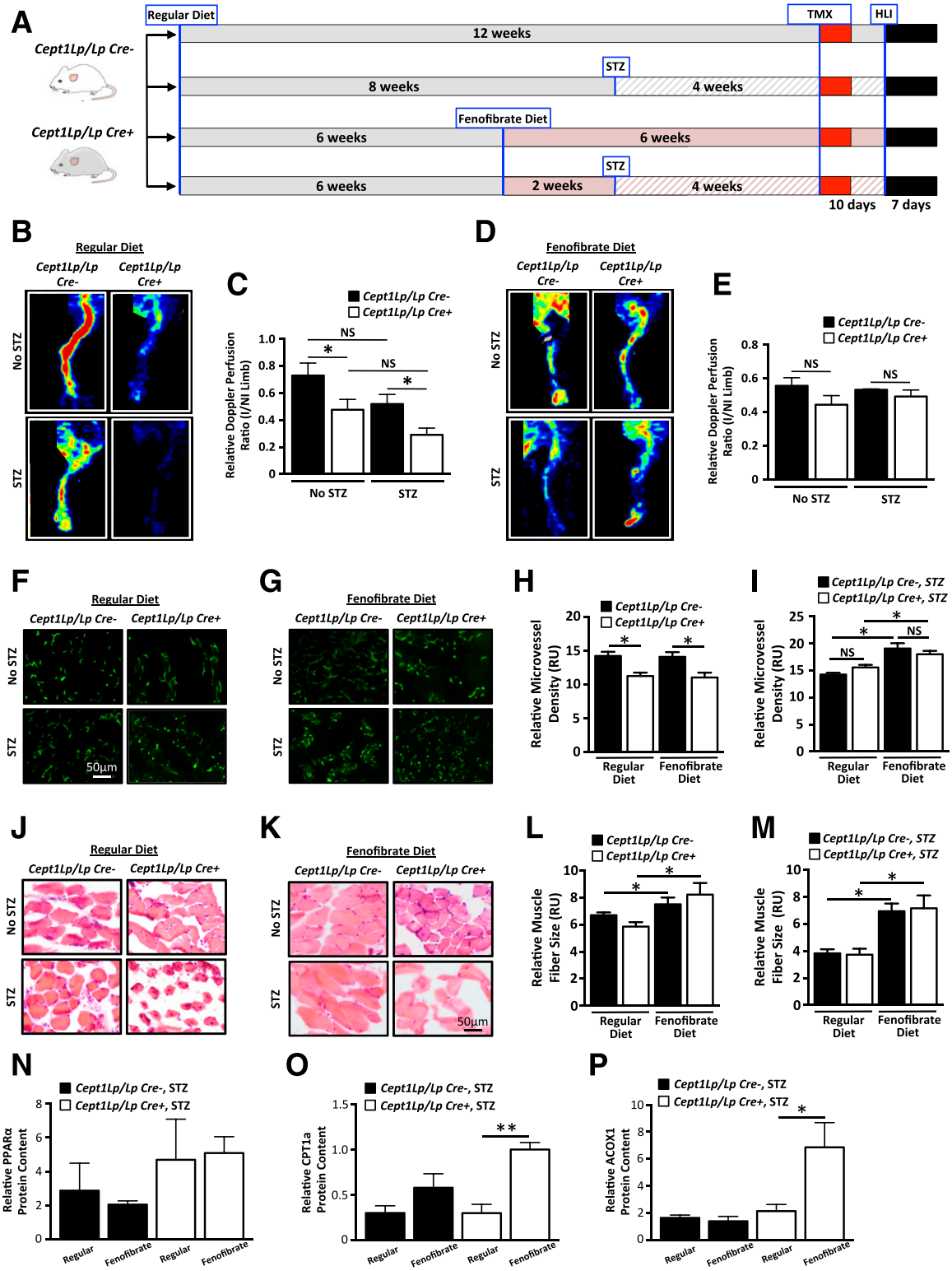

Figure 4—Effect of STZ treatment and fenofibrate diet on HLI recovery in *Cept1Lp/LpCre*$^+$ mice. *A*: *Cept1Lp/LpCre*$^-$ and *Cept1Lp/LpCre*$^+$ mice underwent one of four outlined treatment courses. *B*: Representative Doppler perfusion of ischemic hind limbs of *Cept1Lp/LpCre*$^-$ and *Cept1Lp/LpCre*$^+$ mice treated with or without STZ and maintained on a regular diet. *C*: *Cept1Lp/LpCre*$^+$ mice treated with or without STZ have decreased hind-limb Doppler perfusion (ischemic to nonischemic limb perfusion ratio; n = 4–5 mice per group). *D*: Representative Doppler perfusion of ischemic hind limbs of *Cept1Lp/LpCre*$^-$ and *Cept1Lp/LpCre*$^+$ mice treated with or without STZ and receiving a fenofibrate diet at 6 weeks of age. *E*: *Cept1Lp/LpCre*$^-$ and *Cept1Lp/LpCre*$^+$ mice treated with or without STZ and receiving a fenofibrate diet demonstrated equivalent hind-limb Doppler perfusion (n = 4–15 mice per group). *F*: Representative gastrocnemius microcapillary staining of ischemic hind limbs of *Cept1Lp/LpCre*$^-$ and *Cept1Lp/LpCre*$^+$ mice treated with or without STZ and maintained on a regular or fenofibrate diet. *G*: Representative gastrocnemius microcapillary staining of ischemic hind limbs of *Cept1Lp/LpCre*$^-$ and *Cept1Lp/LpCre*$^+$

mice (Supplementary Fig. 7). In mice pretreated with STZ, fenofibrate diet augmented microvessel density in ischemic hind limbs and abolished differences between *Cept1Lp/LpCre*$^-$ and *Cept1Lp/LpCre*$^+$ mice (Fig. 4*I*). *Cept1Lp/LpCre*$^-$ and *Cept1Lp/LpCre*$^+$ mice that received fenofibrate had preserved skeletal muscle fiber size (less damage) in ischemic hind limbs (Fig. 4*J–L*). Preservation of skeletal muscle fiber size was even more pronounced in *Cept1Lp/LpCre*$^-$ and *Cept1Lp/LpCre*$^+$ mice that were STZ pretreated and received fenofibrate (Fig. 4*J*, *K*, and *M*).

PPARα and its downstream signaling molecules involved in β-fatty acid oxidation were evaluated in the ischemic hind limbs of *Cept1Lp/LpCre*$^-$ and *Cept1Lp/LpCre*$^+$ mice that were pretreated with STZ. Although we observed no difference in PPARα protein content between the mouse groups maintained on a regular or fenofibrate diet (Fig. 4*N* and Supplementary Fig. 8), we observed a robust increase in both CPT1a and ACOX1 in ischemic hind-limb muscle tissue of *Cept1Lp/LpCre*$^+$ mice maintained on a fenofibrate diet (Fig. 4*O* and *P* and Supplementary Fig. 8*B* and *D*).

Fenofibrate Rescues PPARα Activity in the Setting of Cept1 Knockdown

Because we observed that *Cept1Lp/LpCre*$^+$ MLECs treated with fenofibrate had significantly improved tubule formation (Fig. 3*D* and *E* and Supplementary Fig. 9), we aimed to determine whether fenofibrate could also affect PPARα activity in the setting of *Cept1* knockdown. We accomplished this by using *Cept1* esiRNA as an alternative method for acute knockdown of *Cept1* in vitro (Fig. 5*A–C*). HUVECs treated with *Cept1* esiRNA for 36 h had decreased PPARα phosphorylation (Fig. 5*D* and *E*), and treatment of these ECs with fenofibrate for 90 min significantly increased phospho-PPARα (Fig. 5*F* and *G*). Similarly, phospho-PPARα immunostaining was decreased in HUVECs treated with *Cept1* esiRNA (Fig. 5*H* and *I*) and was rescued with fenofibrate treatment (Fig. 5*J* and *K*). Because it has been reported that CEPT1 affects PPARα activity via PC16:0/18:1, we evaluated the impact of *Cept1* knockdown on PC-induced phospho-PPARα levels (Fig. 5*L*). PC16:0/18:1 did not alter *Cept1* or *Ppara* expression (Fig. 5*M* and *N*), but *Cept1* knockdown seemed to significantly blunt PC16:0/18:1-induced PPARα phosphorylation and CPT1a content (Fig. 5*P* and *Q* and Supplementary Fig. 10). The same difference was not observed with PC18:0/18:2 (Fig. 5*P* and *Q*). *Cept1* knockdown also did not affect *Fasn* expression (data not shown).

Postischemia Hind-Limb Perfusion Is Dependent on Ppara and Cept1

ECs isolated from *Ppara*$^{-/-}$ mice demonstrated significantly reduced *Ppara*, *Acox1*, and *Cpt1a* expression (Fig. 6*A–C*). Unilateral femoral artery ligation in *Ppara*$^{-/-}$, *Cept1Lp/LpCre*$^+$, and *Cept1Lp/LpCre*$^+$*Ppara*$^{-/-}$ mice that were maintained on a regular chow diet demonstrated significantly decreased hind-paw perfusion in all groups when compared with *Cept1Lp/LpCre*$^-$ mice (Fig. 6*D* and *E*). However, in mice maintained on chow diet supplemented with fenofibrate, a significant decrease in postischemia day-7 hind-paw perfusion was only observed in *Ppara*$^{-/-}$ mice and *Cept1Lp/LpCre*$^+$*Ppara*$^{-/-}$ mice (Fig. 6*F* and *G*). No difference was observed over a 7-day period between hind-paw perfusion recovery in *Ppara*$^{-/-}$ mice and *Cept1Lp/LpCre*$^+$*Ppara*$^{-/-}$ mice that received regular or fenofibrate diet (Supplementary Fig. 11).

DISCUSSION

The pathometabolic pathways involved in phospholipogenesis play important roles in EC function and recovery after ischemic insults (5,6). Our data support this by demonstrating that CEPT1 has altered expression in the peripheral arterial intima of individuals with diabetes and advanced PAD and is essential for normal EC function and viability and lipid trafficking and synthesis. We also observed that CEPT1 affects PPARα phosphorylation in ECs and that the PPARα agonist fenofibrate can rescue EC function, hind-limb perfusion, and PPARα activation in the setting of reduced *Cept1* expression. These findings confirm that CEPT1 is an important upstream regulator of PPARα and that fenofibrate can influence PPARα activity in ischemic hind limbs, leading to an overall improved phenotype in the setting of diabetes (Fig. 7).

It is commonly understood that diabetes is a strong independent risk factor of PAD and lower-extremity amputations (18,36). In the Framingham cohort, diabetes significantly increased the risk of disabling lower-extremity PAD by 3.5-fold in men and 8.6-fold in women (37).

mice treated with or without STZ and receiving a fenofibrate diet at 6 weeks of age. *H*: Relative microvessel density in ischemic limbs of *Cept1Lp/LpCre*$^-$ and *Cept1Lp/LpCre*$^+$ mice that received either a regular or fenofibrate diet (n = 3–5 mice per group). *I*: Relative microvessel density in ischemic hind limbs of *Cept1Lp/LpCre*$^-$ and *Cept1Lp/LpCre*$^+$ mice treated with or without STZ and maintained on a regular or fenofibrate diet (n = 3–5 mice per group). *J*: Representativehematoxylin-eosin–stained gastrocnemius muscle fiber sections of ischemic hind limbs of *Cept1Lp/LpCre*$^-$ and *Cept1Lp/LpCre*$^+$ mice treated with or without STZ and maintained on a regular diet. *K*: Representative gastrocnemius muscle fiber sections of ischemic hind limbs of *Cept1Lp/LpCre*$^-$ and *Cept1Lp/LpCre*$^+$ mice treated with or without STZ and receiving a fenofibrate diet at 6 weeks of age. *L*: Relative muscle fiber size in ischemic limbs of *Cept1Lp/LpCre*$^-$ and *Cept1Lp/LpCre*$^+$ that received either a regular or fenofibrate diet (n = 3 mice per group). *M*: Relative muscle fiber size in ischemic limbs of *Cept1Lp/LpCre*$^-$ and *Cept1Lp/LpCre*$^+$ mice that received STZ and a regular or fenofibrate diet (n = 3 mice per group). *N–P*: Quantified Western blot analysis of PPARα (*N*), CPT1a (*O*), and ACOX1 (*P*) in *Cept1Lp/LpCre*$^-$ and *Cept1Lp/LpCre*$^+$ mice that received STZ treatment (n = 3 per sample). *P < 0.05; **P < 0.01. I/NI, ischemic/non-ischemic; RU, relative unit.

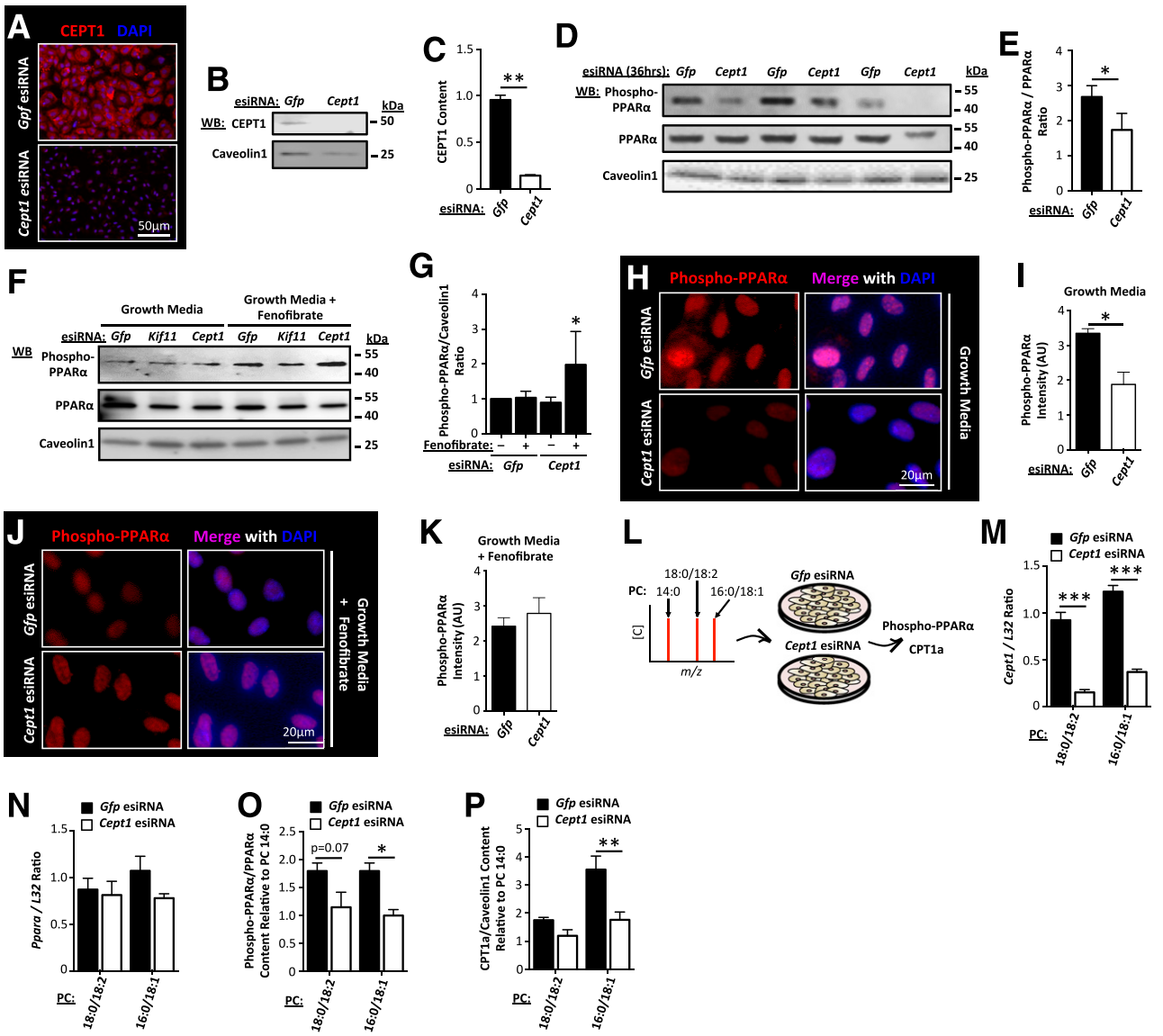

Figure 5—Fenofibrate rescues PPARα phosphorylation after acute knockdown of *Cept1*, and CEPT1 is essential for 16:0/18:1 activation of PPARα. *A*: Immunostaining of HUVECs treated with *Gfp* or *Cept1* esiRNA. *B*: Representative Western blot (WB) of CEPT1 and caveolin-1 loading control in HUVECs treated with *Gfp* or *Cept1* esiRNA. *C*: Relative content of CEPT1 in HUVECs treated with *Gfp* or *Cept1* esiRNA (n = 3 per condition). *D*: Representative WB of phospho-PPARα, total PPARα, and caveolin-1 loading control in HUVECs treated with *Gfp* or *Cept1* esiRNA for 36 h (n = 3 shown per condition). *E*: Ratio of phospho-PPARα to PPARα in HUVECs treated with *Gfp* or *Cept1* esiRNA (n = 3 per condition). *F*: Representative WB of phospho-PPARα, total PPARα, and caveolin-1 loading control in HUVECs treated with *Gfp* or *Cept1* esiRNA and with or without fenofibrate for 90 min. *G*: Ratio of phospho-PPARα to cavolin-1 in HUVECs treated with *Gfp* or *Cept1* esiRNA (n = 5 per condition). *H*: Representative immunostains of phospho-PPARα in HUVECs treated with *Gfp* or *Cept1* esiRNA and maintained in growth media. *I*: Quantification of phospho-PPARα intensity in HUVECs treated with *Gfp* or *Cept1* esiRNA and maintained in growth media (n = 4–5 per condition). *J*: Representative immunostains of phospho-PPARα in HUVECs treated with *Gfp* or *Cept1* esiRNA and maintained in growth media supplemented with 50 μmol/L fenofibrate. *K*: Quantification of phospho-PPARα intensity in HUVECs treated with *Gfp* or *Cept1* esiRNA and maintained in growth media supplemented with 50 μmol/L fenofibrate (n = 5–6 per condition). *L*: HUVECs treated with *Gfp* or *Cept1* esiRNA were also treated with PC18:0/18:2 or PC16:0/18:1 and relative content of phospho-PPARα and CPT1a evaluated. *M* and *N*: *Cept1* (*M*) and *Ppara* (*N*) expression in HUVECs treated with different PC and esiRNA conditions (n = 3 per condition). *O* and *P*: Relative to PC14:0 treatments, the ratios of phospho-PPARα to total PPARα (*O*) and CPT1a to caveolin-1 loading control (*P*) are demonstrated in HUVECs treated with *Gfp* or *Cept1* esiRNA and PC18:0/18:2 or PC16:0/18:1. *$P < 0.05$; **$P < 0.01$; ***$P < 0.001$. AU, arbitrary unit.

Similarly, other studies have confirmed increased prevalence of advanced PAD in individuals with diabetes and increased risk of amputation despite attempted interventions to improve lower-extremity arterial perfusion (36,38–41). To date, the FIELD study is the only study that has demonstrated a relative risk reduction in amputations in individuals with diabetes (23,42). That study demonstrated that patients with diabetes who were randomly assigned to fenofibrate had a significant 43% reduction in any first amputation and 61% decrease in minor (below the

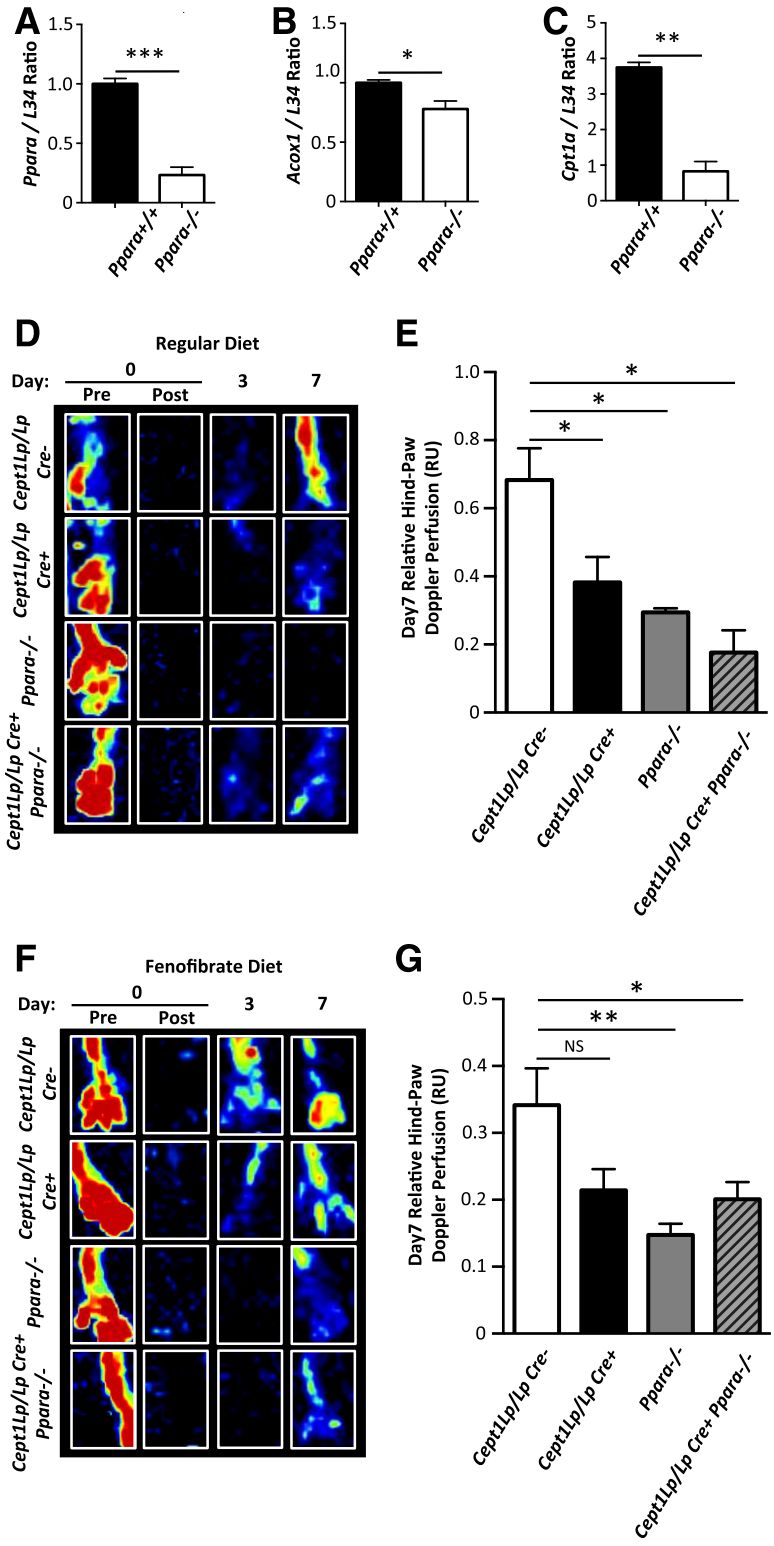

Figure 6—*Ppara* is essential for fenofibrate rescue of ischemic hind-paw Doppler perfusion. *A–C*: Expression of *Ppara*, (*A*) *Acox1*, (*B*) and *Cpt1a* (C) in MLECs isolated from $Ppara^{+/+}$ and $Ppara^{-/-}$ mice ($n = 3$ per condition from ECs pooled from three mice per genotype). *D*: Representative hind-paw perfusion at baseline pre-HLI (day 0) and post-HLI days 3 and 7 in $Cept1Lp/LpCre^{-}$, $Cept1Lp/LpCre^{+}$, $Ppara^{-/-}$, and $Cept1Lp/LpCre^{+}Ppara^{-/-}$ mice maintained on a regular diet. *E*: Quantitative assessment of relative hind-paw Doppler perfusion across the different mouse genotypes maintained on a regular diet ($n = 4–10$ mice per genotype). *F*: Representative hind-paw perfusion of different genotypes of mice that received a fenofibrate diet. *G*: Quantitative assessment of relative hind-paw Doppler perfusion across the different genotypes of mice that received a fenofibrate diet ($n = 10–15$ mice per genotype). $^{*}P < 0.05$; $^{**}P < 0.01$; $^{***}P < 0.001$.

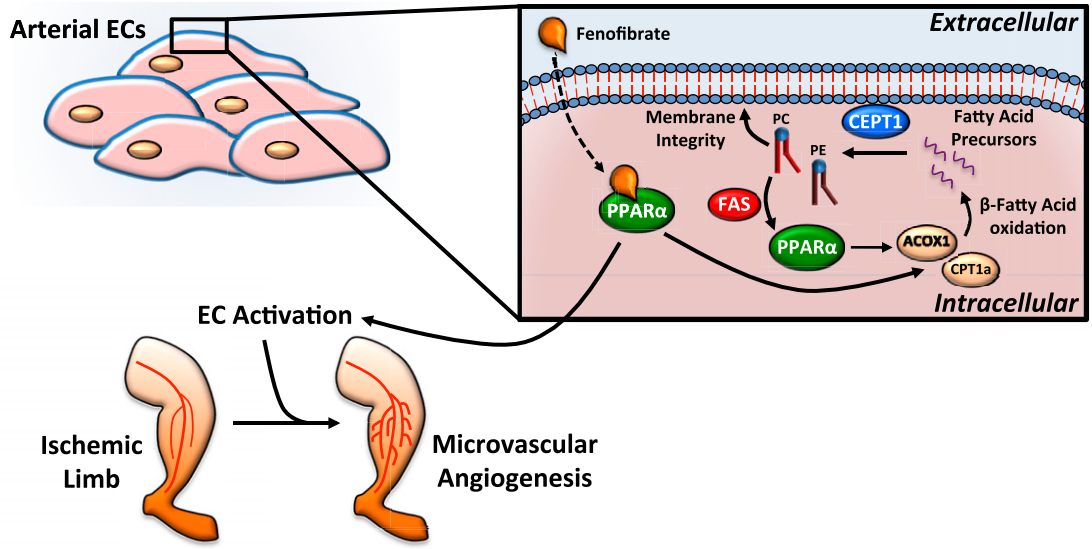

Figure 7—Role of CEPT1 and fenofibrate in PPARα activation. In endothelium, CEPT1 generates PCs and PEs from fatty acid precursors via phospholipogenesis. PCs and PEs are essential for various cellular functions, including membrane integrity and activation of transcription factors such as PPARα. PPARα phosphorylation is dependent on CEPT1 and is also induced by fenofibrate treatment. PPARα activation leads to increased β-fatty acid oxidation enzymes, such as ACOX1 and CPT1a. PPARα expression seems to be essential for EC activation and appropriate recovery response to peripheral-limb ischemia and microvascular angiogenesis. FAS, fatty acid synthase.

ankle) amputations (23). The mechanism of action that confers this notable clinical benefit in individuals with diabetes has remained up for debate, with various reports arguing the impact of fenofibrate on PPARα-dependent and -independent signaling pathways (43–45).

We previously reported that diabetes adversely affects phospholipid and CEPT1 content in human carotid artery endarterectomy plaques (24). Prearachidonic acid pPEs derived from the CEPT1-catalyzed Kennedy pathway were observed to be among the highest phospholipids present in the carotid plaque of patients with diabetes. Similarly, in this study, we observed that CEPT1 content was also increased in a moderate-size cohort of patients with diabetes and lower-extremity atherosclerotic occlusive disease. Interestingly, CEPT1 content was also elevated relative to the extent of arterial occlusive disease severity, with Max diseased arterial intima containing higher levels of CEPT1 and downstream PCs and PEs. Because we observed that CEPT1 was also essential for EC function and normal recovery of murine ischemic hind limbs, it is likely that its abundance in diseased peripheral arterial segments of patients with diabetes is reflective of a possible healing and/or compensatory mechanism.

Previously, it was demonstrated that in liver tissue, CEPT1-derived PC (PC16:0/18:1) is an essential ligand for PPARα activation and PPARα-dependent gene expression (16). Binding of this CEPT1-derived PC to PPARα is promoted by other lipid mediators, such as fatty acid synthase, and displaced by PPARα agonist Wy14,643. In this study, we observed similar findings in ECs and demonstrated that PPARα-dependent gene expression in ECs required *Cept1* expression. *Cept1* expression also seemed necessary to facilitate PC16:0/18:1-induced phosphorylation and activation of PPARα. Moreover, *Cept1Lp/Lp* MLECs had reduced *Acox1* and *Cpt1a* expression, and acute knockdown of *Cept1* with siRNA also led to reduced phospho-PPARα levels. These findings confirm that CEPT1 plays an important upstream role in PPARα activation of β-oxidative lipid metabolism in ECs.

A growing body of evidence has demonstrated that disruption of CEPT1 is associated with a variety of human conditions. CEPT1 plays important roles in cellular lipid droplet formation (14), parasitic invasions (1), and virulence (3). Recent genome-wide association studies have also identified specific human phenotypes that are related to CEPT1 polymorphisms (13,46). Genetic deletion of enzymes immediately proximal to CEPT1 in the Kennedy pathway leads to lethal phenotypes early in embryogenesis (47). Our study adds to our understanding of the importance of CEPT1 in cellular metabolism and demonstrates that CEPT1 is essential for EC activation and function. Additionally, CEPT1 seems essential for ischemia-induced microvascular angiogenesis and ischemic hind-limb perfusion and skeletal muscle recovery. In mice treated with STZ to induce a diabetes-like phenotype (28,30), knockdown of CEPT1 seemed to exacerbate hind-limb malperfusion. Although STZ-induced diabetes is not entirely representative of the complex metabolic mechanisms associated with T2D in humans, these observations highlight the importance of CEPT1 in EC homeostasis in the setting of ischemia and a diabetes-like phenotype. Because patients with diabetes and advanced PAD have higher CEPT1 content in the arterial intima, next steps would be to determine the impact of CEPT1 knockdown in mouse models

with a diet- or gene-induced T2D-like phenotype and examine whether CEPT1 knockdown in other cell types (e.g., smooth muscle cells or myeloid cells) manifests with similar impairments in postischemia hind-limb perfusion and recovery.

There is conflicting evidence regarding the effect of fenofibrate on ECs (43,48). In a randomized placebo-controlled trial, treatment with fenofibrate improved EC-dependent vascular reactivity over a 12-week period and reduced markers for EC dysfunction, including tumor necrosis factor-α, interleukin-1β, and interleukin-6 in plasma (48). Similar to our study, fenofibrate was previously shown to decrease ischemia-induced tissue damage (48). For example, in retinal tissue, fenofibrate was observed to activate AMP kinase in ECs via a PPARα-independent pathway (49) and possibly to also induce nitric oxide synthesis (50). However, others have reported that fenofibrate can actually decrease EC function and inhibit tumor-induced angiogenesis (43). It is likely that variable effects of fenofibrate on PPARα-dependent and -independent signaling mechanisms are in part responsible for the differential responses observed in different tissue beds. In our study, we demonstrated that fenofibrate rescued phospho-PPARα in ECs treated with *Cept1* siRNA. Although fenofibrate partially rescued perfusion in hind limbs of *Cept1Lp/Lp* mice, it did not seem to have the same effect on *Ppara*$^{-/-}$ or *Cept1Lp/LpPpara*$^{-/-}$ mice. This suggests that the observed effects of fenofibrate in ECs and ischemic hind limbs were at least in part PPARα dependent.

In conclusion, we report that CEPT1 and its downstream phospholipids are present in high levels in the arterial intima of patients with T2D and advanced PAD. We also observed that CEPT1 was essential for EC function and normal tissue recovery after ischemia. Fenofibrate seemed to rescue CEPT1-mediated activation of PPARα and perfusion of ischemic hind limbs in a PPARα-dependent fashion. These findings confirm the regulatory effects of CEPT1 upstream of PPARα and provide further insight into the mechanisms of action of fenofibrate in ECs, diabetes, and peripheral ischemia.

Acknowledgments. The authors thank Amanda Penrose, Section of Vascular Surgery at Washington University, for assistance with collection, preparation, and processing of Biobank Core Facility research samples and Susan Grathwohl, Section of Vascular Surgery at Washington University, for mouse colony maintenance and independent review of peripheral murine angiograms. The authors thank Dr. Chenglong Li, Section of Vascular Surgery at Washington University, for assistance with *Ppara*$^{-/-}$ murine HLI operations. *VE-Cadherin-CreERT2* mice were a gift from the laboratory of Dr. Ralf Adams, Max Planck Institute for Molecular Biomedicine, Germany. The authors also thank Dr. Xiaochao Wei, Division of Endocrinology, Metabolism, and Lipid Research at Washington University, and Dr. Rithwick Rajagopal, Division of Endocrinology, Metabolism, and Lipid Research at Washington University, for their critical suggestions and critiques.

Funding. This work was supported by the Washington University School of Medicine Vascular Surgery Biobank Core Facility and by the Vascular Cures Foundation Wylie Scholar Award (M.A.Z.), the American Surgical Association Research Fellowship Award (M.A.Z.), the Society for Vascular Surgery Foundation Research Investigator Award (M.A.Z.), Washington University School of Medicine Diabetes Research Center National Institutes of Health (NIH)/National Institute of Diabetes and Digestive and Kidney Diseases (NIDDK) grants P30 DK020589 (M.A.Z.), NIH/National Heart, Lung, and Blood Institute grant K08 HL132060 (M.A.Z.), Nutrition Obesity Research Center NIH/NIDDK grant P30 DK056341 (B.W.P.), and NIH/NIDDK grant R01 DK101392 (C.F.S.). The Washington University School of Medicine Mass Spectrometry Facility is supported by U.S. Public Health Service grants P41-GM103422 and P60-DK-20579.

Duality of Interest. No potential conflicts of interest relevant to this article were reported.

Author Contributions. M.A.Z. and C.F.S. were responsible for conception and design. M.A.Z., X.J., C.Y., L.B., K.D., N.H., O.S., B.W.P., and C.F.S. analyzed and interpreted data. X.J., C.Y., L.B., K.D., N.H., O.S., B.W.P., and F.-F.H. collected data. M.A.Z., X.J., and C.F.S. wrote the manuscript. M.A.Z. and C.F.S. critically revised the manuscript. M.A.Z., X.J., C.Y., L.B., K.D., N.H., O.S., B.W.P., F.-F.H., and C.F.S. provided final approval of the manuscript. M.A.Z., X.J., C.Y., K.D., and C.F.S. performed statistical analysis. M.A.Z. obtained funding and had overall responsibility. C.E. contributed to analysis and interpretation, collection of data, and provided final approval of the manuscript. M.A.Z. is the guarantor of this work and, as such, has full access to all the data in the study and takes responsibility for the integrity of the data and the accuracy of the data analysis.

References

1. Déchamps S, Wengelnik K, Berry-Sterkers L, Cerdan R, Vial HJ, Gannoun-Zaki L. The Kennedy phospholipid biosynthesis pathways are refractory to genetic disruption in Plasmodium berghei and therefore appear essential in blood stages. Mol Biochem Parasitol 2010;173:69–80

2. Gibellini F, Smith TK. The Kennedy pathway–de novo synthesis of phosphatidylethanolamine and phosphatidylcholine. IUBMB Life 2010;62:414–428

3. Moessinger C, Klizaite K, Steinhagen A, et al. Two different pathways of phosphatidylcholine synthesis, the Kennedy pathway and the Lands cycle, differentially regulate cellular triacylglycerol storage. BMC Cell Biol 2014;15:43

4. Funai K, Song H, Yin L, et al. Muscle lipogenesis balances insulin sensitivity and strength through calcium signaling. J Clin Invest 2013;123:1229–1240

5. Ma W, Wu JH, Wang Q, et al. Prospective association of fatty acids in the de novo lipogenesis pathway with risk of type 2 diabetes: the Cardiovascular Health Study. Am J Clin Nutr 2015;101:153–163

6. Wei X, Schneider JG, Shenouda SM, et al. De novo lipogenesis maintains vascular homeostasis through endothelial nitric-oxide synthase (eNOS) palmitoylation. J Biol Chem 2011;286:2933–2945

7. Henneberry AL, Wistow G, McMaster CR. Cloning, genomic organization, and characterization of a human cholinephosphotransferase. J Biol Chem 2000;275:29808–29815

8. Wright MM, McMaster CR. PC and PE synthesis: mixed micellar analysis of the cholinephosphotransferase and ethanolaminephosphotransferase activities of human choline/ethanolamine phosphotransferase 1 (CEPT1). Lipids 2002;37:663–672

9. Koch HB, Zhang R, Verdoodt B, et al. Large-scale identification of c-MYC-associated proteins using a combined TAP/MudPIT approach. Cell Cycle 2007;6:205–217

10. Lagace TA. Phosphatidylcholine: greasing the cholesterol transport machinery. Lipid Insights 2016;8(Suppl. 1):65–73

11. Baxter AA, Hulett MD, Poon IK. The phospholipid code: a key component of dying cell recognition, tumor progression and host-microbe interactions. Cell Death Differ 2015;22:1893–1905

12. Ahmed MY, Al-Khayat A, Al-Murshedi F, et al. A mutation of EPT1 (SELENOI) underlies a new disorder of Kennedy pathway phospholipid biosynthesis. Brain 2017;140:547–554

13. Gao C, Langefeld CD, Ziegler JT, et al. Genome-wide study of subcutaneous and visceral adipose tissue reveals novel sex-specific adiposity loci in Mexican Americans. Obesity (Silver Spring) 2018;26:202–212
14. Krahmer N, Guo Y, Wilfling F, et al. Phosphatidylcholine synthesis for lipid droplet expansion is mediated by localized activation of CTP: phosphocholine cytidylyltransferase. Cell Metab 2011;14:504–515
15. Mangelsdorf DJ, Thummel C, Beato M, et al. The nuclear receptor superfamily: the second decade. Cell 1995;83:835–839
16. Chakravarthy MV, Lodhi IJ, Yin L, et al. Identification of a physiologically relevant endogenous ligand for PPARalpha in liver. Cell 2009;138:476–488
17. Desvergne B, Wahli W. Peroxisome proliferator-activated receptors: nuclear control of metabolism. Endocr Rev 1999;20:649–688
18. Beckman JA, Creager MA, Libby P. Diabetes and atherosclerosis: epidemiology, pathophysiology, and management. JAMA 2002;287:2570–2581
19. Resnick HE, Shorr RI, Kuller L, Franse L, Harris TB. Prevalence and clinical implications of American Diabetes Association-defined diabetes and other categories of glucose dysregulation in older adults: the health, aging and body composition study. J Clin Epidemiol 2001;54:869–876
20. Ruiter MS, van Golde JM, Schaper NC, Stehouwer CD, Huijberts MS. Diabetes impairs arteriogenesis in the peripheral circulation: review of molecular mechanisms. Clin Sci (Lond) 2010;119:225–238
21. Zayed M, Bech F, Hernandez-Boussard T. National review of factors influencing disparities and types of major lower extremity amputations. Ann Vasc Surg 2014;28:1157–1165
22. International Diabetes Federation. *Diabetes and Foot Care: Time to Act*. Brussels, Belgium, International Diabetes Federation, 2005
23. Rajamani K, Colman PG, Li LP, et al.; FIELD Study Investigators. Effect of fenofibrate on amputation events in people with type 2 diabetes mellitus (FIELD study): a prespecified analysis of a randomised controlled trial. Lancet 2009;373:1780–1788
24. Zayed MA, Hsu FF, Patterson BW, et al. Diabetes adversely affects phospholipid profiles in human carotid artery endarterectomy plaques. J Lipid Res 2018;59:730–738
25. Monvoisin A, Alva JA, Hofmann JJ, Zovein AC, Lane TF, Iruela-Arispe ML. VE-cadherin-CreERT2 transgenic mouse: a model for inducible recombination in the endothelium. Dev Dyn 2006;235:3413–3422
26. Wei X, Adak S, Zayed M, et al. Endothelial palmitoylation cycling coordinates vessel remodeling in peripheral artery disease. Circ Res 2020;127:249–265
27. Zayed MA, Yuan W, Leisner TM, et al. CIB1 regulates endothelial cells and ischemia-induced pathological and adaptive angiogenesis. Circ Res 2007;101:1185–1193
28. Zayed MA, Wei X, Park KM, et al. *N*-acetylcysteine accelerates amputation stump healing in the setting of diabetes. FASEB J 2017;31:2686–2695
29. Rueden CT, Schindelin J, Hiner MC, et al. ImageJ2: ImageJ for the next generation of scientific image data. BMC Bioinformatics 2017;18:529
30. Xin R, An D, Li Y, Fu J, Huang F, Zhu Q. Fenofibrate improves vascular endothelial function in diabetic mice. Biomed Pharmacother 2019;112:108722
31. Livak KJ, Schmittgen TD. Analysis of relative gene expression data using real-time quantitative PCR and the 2(-delta delta C(T)) method. Methods 2001;25:402–408
32. Hsu FF. Complete structural characterization of ceramides as $[M-H]^-$ ions by multiple-stage linear ion trap mass spectrometry. Biochimie 2016;130:63–75
33. Hsu FF, Kuhlmann FM, Turk J, Beverley SM. Multiple-stage linear ion-trap with high resolution mass spectrometry towards complete structural characterization of phosphatidylethanolamines containing cyclopropane fatty acyl chain in Leishmania infantum. J Mass Spectrom 2014;49:201–209
34. Hsu FF, Turk J. Electrospray ionization/tandem quadrupole mass spectrometric studies on phosphatidylcholines: the fragmentation processes. J Am Soc Mass Spectrom 2003;14:352–363
35. Hsu FF, Turk J. Electrospray ionization with low-energy collisionally activated dissociation tandem mass spectrometry of glycerophospholipids: mechanisms of fragmentation and structural characterization. J Chromatogr B Analyt Technol Biomed Life Sci 2009;877:2673–2695
36. Jude EB, Oyibo SO, Chalmers N, Boulton AJ. Peripheral arterial disease in diabetic and nondiabetic patients: a comparison of severity and outcome. Diabetes Care 2001;24:1433–1437
37. Abbott RD, Brand FN, Kannel WB. Epidemiology of some peripheral arterial findings in diabetic men and women: experiences from the Framingham study. Am J Med 1990;88:376–381
38. Beks PJ, Mackaay AJ, de Neeling JN, de Vries H, Bouter LM, Heine RJ. Peripheral arterial disease in relation to glycaemic level in an elderly Caucasian population: the Hoorn study. Diabetologia 1995;38:86–96
39. Faries PL, LoGerfo FW, Hook SC, et al. The impact of diabetes on arterial reconstructions for multilevel arterial occlusive disease. Am J Surg 2001;181:251–255
40. Feinglass J, Pearce WH, Martin GJ, et al. Postoperative and amputation-free survival outcomes after femorodistal bypass grafting surgery: findings from the Department of Veterans Affairs National Surgical Quality Improvement Program. J Vasc Surg 2001;34:283–290
41. Shammas AN, Jeon-Slaughter H, Tsai S, et al. Major limb outcomes following lower extremity endovascular revascularization in patients with and without diabetes mellitus. J Endovasc Ther 2017;24:376–382
42. Keech A, Simes RJ, Barter P, et al.; FIELD Study Investigators. Effects of long-term fenofibrate therapy on cardiovascular events in 9795 people with type 2 diabetes mellitus (the FIELD study): randomised controlled trial. Lancet 2005;366:1849–1861
43. Panigrahy D, Kaipainen A, Huang S, et al. PPARalpha agonist fenofibrate suppresses tumor growth through direct and indirect angiogenesis inhibition. Proc Natl Acad Sci U S A 2008;105:985–990
44. Katayama A, Yamamoto Y, Tanaka K, et al. Fenofibrate enhances neovascularization in a murine ischemic hindlimb model. J Cardiovasc Pharmacol 2009;54:399–404
45. Yuan J, Tan JTM, Rajamani K, et al. Fenofibrate rescues diabetes-related impairment of ischemia-mediated angiogenesis by PPARα-independent modulation of thioredoxin-interacting protein. Diabetes 2019;68:1040–1053
46. Christophersen IE, Magnani JW, Yin X, et al. Fifteen genetic loci associated with the electrocardiographic P wave. Circ Cardiovasc Genet 2017;10:e001667
47. Wu G, Aoyama C, Young SG, Vance DE. Early embryonic lethality caused by disruption of the gene for choline kinase alpha, the first enzyme in phosphatidylcholine biosynthesis. J Biol Chem 2008;283:1456–1462
48. Ryan KE, McCance DR, Powell L, McMahon R, Trimble ER. Fenofibrate and pioglitazone improve endothelial function and reduce arterial stiffness in obese glucose tolerant men. Atherosclerosis 2007;194:e123–e130
49. Kim J, Ahn JH, Kim JH, et al. Fenofibrate regulates retinal endothelial cell survival through the AMPK signal transduction pathway. Exp Eye Res 2007;84:886–893
50. Murakami H, Murakami R, Kambe F, et al. Fenofibrate activates AMPK and increases eNOS phosphorylation in HUVEC. Biochem Biophys Res Commun 2006;341:973–978